A volume penalization lattice Boltzmann method for simulating flows in the presence of obstacles

M. Benamour, Erwan Liberge, C. Béghein

Version of Record: https://www.sciencedirect.com/science/article/pii/S1877750319303771
Manuscript_30fb4f5802dd3e1cf42b725e7dcab224

A volume penalization lattice Boltzmann method for simulating flows in the presence of obstacles

M. Benamour[a,1], E. Liberge[b,1], C. Béghein[b,1,*]

[a] *CESI, 93 boulevard de la Seine BP602, 92006 Nanterre, France*
[b] *LaSIE, UMR 7356 CNRS, La Rochelle Université, av. M. Crépeau, 17042 La Rochelle Cedex 1, France*

Abstract

The LBM is combined with the Volume Penalization (VP LBM) approach to simulate flows in the presence of obstacles. The single relaxation time LBM and the multiple relaxation time LBM are used. The approach is evaluated for various test cases: flows enhanced by moving boundaries for which an analytical solution is known, flow past a cylinder at a Reynolds number of 500, and flow induced vibration of a cylinder. A comparison of our results with analytical results and with results found in the literature, demonstrates the reliability of the VP LBM to treat complex flows.

Keywords: Lattice Boltzmann method, Volume penalization, Navier–Stokes equations

1. Introduction

The approach proposed in this paper consists in coupling the Lattice Boltzmann Method (LBM) with the Volume Penalization (VP) technique to model fluid flows in the presence of obstacles, and more particularly moving obstacles. To compute such flows, it is necessary to use fine grids and small time steps, and this leads to a high amount of computing time when classical numerical approaches are used to solve the Navier-Stokes equations (finite differences, finite volumes, finite elements). An important advantage of the lattice Boltzmann method is that it can be efficiently parallelized on graphic processor units (GPUs) [1, 2], which enables a substantial decrease in computational time. The lattice Boltzmann method has been widely used for fluid flow simulation [3, 4]. In literature, one can notice that various approaches have been implemented in a lattice Boltzmann framework to model flows around obstacles.

In 1994, Ladd [5] adapted the bounce back method to the computation of flows around moving particles, and he proposed the momentum exchange approach to evaluate the hydrodynamic force acting on the particle. To treat curved boundaries, other authors improved this method by introducing interpolation formula into the bounce back rule [6, 7, 8]. Filippova and Hänel [9], Mei et al. [10], Guo et al. [11] developed a bounce back method

*Corresponding author. Tel 33 5 46 45 82 37, Fax 33 5 46 45 82 41
Email addresses: mbenamour@cesi.fr (M. Benamour), erwan.liberge@univ-lr.fr (E. Liberge), claudine.beghein@univ-lr.fr (C. Béghein)
[1] Authors make equal contributions.

based on the construction of an equilibrium distribution function at the solid node, where extrapolations were used to calculate the velocity at the solid node. Noble and Torczynski [12] modified the lattice Boltzmann equation, by introducing a source term in the collision term. With this method, the Single Relaxation Time Lattice Boltzmann equation could be solved both in the fluid region, and in regions occupied by a solid obstacle (where the Zou and He bounce back rule [13] was applied thanks to this source term).

The immersed boundary method becomes more and more popular in the lattice Boltzmann community [14, 15, 16, 17, 18]. It consists in solving the Navier-Stokes equations with a source term that mimics the influence of the boundary on the flow, on a fixed Eulerian mesh. The solid boundary (the immersed boundary) is tracked using a Lagrangian approach [19]. This method works well for deformable bodies (elastic particles for instance [20, 21, 22]). Nevertheless, it is a bit more complicated to treat solid bodies when using the immersed boundary method. Feng and Michaelides [23] and Ten Cate et al. [24] were the first authors to combine this technique with the lattice Boltzmann method to simulate flows around moving rigid particles. In these initial works, the solid boundary was modeled with Lagrangian marker points connected by an elastic spring whose constant needed to be empirically adjusted to make the boundary rigid. To circumvent this difficulty, Feng and Michaelides [25] and Dupuis et al. [26] coupled the direct forcing immersed boundary method developed by Fadlun et al. [27] in a finite difference formulation, with the lattice Boltzmann method. However, with the immersed boundary method, the force that represents the influence of the immersed boundary on the fluid, is applied to the Eulerian fluid nodes surrounding the immersed boundary, and the no-slip boundary condition is not exactly satisfied at the fluid solid interface. To improve that method, Wu and Shu [28] developed a variant of the immersed boundary lattice Boltzmann method based on an implicit correction of the velocity calculated on the Eulerian nodes in the vicinity of the immersed boundary. With that method, the no-slip boundary condition is satisfied at the fluid solid interface.

Meldi et al. [29] applied the Arbitrary Lagrangian Eulerian (ALE) approach in a lattice Boltzmann framework. The ALE technique consists in combining the Eulerian technique far from the moving obstacle, and the Lagrangian technique in the vicinity of the obstacle. In the fluid region near the obstacle, the conservation equations are written on a mesh that moves arbitrarily according to time [30, 31]. This implies an increase in computing time. The Distributed Lagrange Multiplier Fictitious Domain (DLM/FD) method was also coupled with the LBM to calculate flows around deforming bodies [32]. This work was based on the DLM/FD method developed by Glowinski et al. [33] (for rigid body motion) and extended to deforming bodies by Yu [34]. The DLM/FD method consists in writing the governing equations on a fixed domain, including the fluid and the solid regions, and using Lagrange multipliers (or pseudo body forces) to make the fictitious fluid in the solid region move like the solid medium. With this method the costly re-meshing step is avoided.

Fluid Structure Interaction (FSI) problems can be tackled with the volume penalization technique by extending the Navier-Stokes equations to the whole domain (fluid domain and solid domain), and penalizing the solid domain. While a Lagrange multiplier (a body force) makes the fluid inside the solid region move as the solid medium with the DLM/FD

method, with the VP method, a body force term is added to the Navier-Stokes equations, which enables to consider the solid domain as a porous medium that moves at the same velocity as the solid velocity. Furthermore, with this method, it is not necessary to apply a boundary condition for the pressure at the fluid-solid interface. Since the whole domain (fluid and solid) is treated as a porous medium with a very low permeability inside the solid medium, and a very high one inside the fluid medium, the pressure adapts naturally when lattice nodes cross the boundary (a refilling algorithm as required for several bounce back methods [35] is not needed), when dealing with flows around moving bodies. This is also the case for other methods, such as the method proposed by Noble and Torczynski [12], or the immersed boundary method. However, unlike with the Lagrange multiplier method, the FSI problems that can be tackled with the volume penalization method involve only rigid body motions. The Volume Penalization method is efficient for fixed Cartesian grids, and it avoids the re meshing step necessary in classical approaches devoted to Fluid Structure Interaction modeling [36, 31]. The promising results obtained with the Volume Penalization technique combined with various solving approaches (finite element method, finite volume method, spectral method, vortex method) [37, 38, 39, 40, 41] make the volume penalization method a good candidate to be coupled with LBM for modeling fluid structure interaction problems. In contrast with the classical immersed boundary methods, the convergence of the volume penalization method has been mathematically proved [37]. To the authors' knowledge, this method has not yet been developed in a lattice Boltzmann framework.

In a previous paper [42, 43], we successfully applied the combined Volume Penalization Lattice Boltzmann Method (VP-LBM) to flows around motionless obstacles, for relatively low Reynolds numbers (less or equal than 100). The Single Relaxation Time Lattice Boltzmann Method was used. In this work, we combined the Multi Relaxation Time Lattice Boltzmann Method with the Volume Penalization approach, and we simulated more complex flows: flows created by moving boundaries for which an analytical solution is known (an asymmetric flow and a flow between two concentric cylinders), an unsteady flow past a cylinder at a Reynolds number of 500, and the flow induced vibration of a cylinder at a Reynolds number of 100. For these two latter more complex cases, the VP LBM method, which is easy to implement, was parallelized. In the following paragraph, the Lattice Boltzmann method combined with the volume penalization technique will be described. Then, the numerical results obtained for the test cases will be presented. In the last paragraph of the paper, concluding remarks will be given.

2. Governing equations

2.1. Fluid flow computation

When solving fluid structure interaction problems using a volume penalization technique, a source term involving the influence of the obstacle on the fluid flow is introduced into the Navier-Stokes equations. The incompressible Navier-Stokes equations with a source term, and the continuity equation read:

$$\begin{aligned} &\rho\frac{\partial \boldsymbol{u}}{\partial t} + \rho\boldsymbol{u}\cdot\nabla\boldsymbol{u} = -\nabla p + \mu\nabla^2\boldsymbol{u} + \boldsymbol{f} \\ &\nabla\cdot\boldsymbol{u} = 0 \end{aligned} \tag{1}$$

where ρ and μ are the density and the dynamic viscosity of the fluid considered, p and $\boldsymbol{u}$ are the pressure and the velocity, $\boldsymbol{f}$ is a body force that mimics the influence of the obstacle on the fluid flow. In this article, the lattice Boltzmann method was chosen for fluid flow computation. The lattice Boltzmann method consists in solving a simplified version of the Boltzmann equation on a lattice, where fluid parcels move according to a finite set of prescribed velocities. The correspondence between the lattice Boltzmann equation (mesoscopic level) and the Navier-Stokes equations (macroscopic level) is achieved thanks to the Chapman Enskog procedure.

2.1.1. Single Relaxation Time LBM

This model is based on a linear collision operator, proposed by Bhatnagar, Gross and Krook (BGK) [3, 4]. The lattice Boltzmann equation with a forcing term is expressed as:

$$f_\alpha(\boldsymbol{x}+\boldsymbol{\xi}_\alpha\Delta t, t+\Delta t) - f_\alpha(\boldsymbol{x},t) = -\frac{1}{\tau}(f_\alpha(\boldsymbol{x},t) - f_\alpha^{eq}(\boldsymbol{x},t)) + \Delta t F_\alpha \tag{2}$$

where f_α is the distribution function along the α direction, $\boldsymbol{\xi_\alpha}$ is the particle velocity, f_α^{eq} is the equilibrium distribution function, τ is the non-dimensional relaxation time, Δt is the time step, and F_α is a forcing term that corresponds to the source term $\boldsymbol{f}$. The nine-velocity square lattice model $D2Q9$ shown in figure 1 was chosen. In this model, the lattice velocities are:

$$\boldsymbol{\xi}_\alpha = \begin{cases} (0,0), & \alpha = 0 \\ (cos[(\alpha-1)\pi/2], sin[(\alpha-1)\pi/2])c, & \alpha = 1,2,3,4 \\ (cos[(2\alpha-9)\pi/4], sin[(2\alpha-9)\pi/4])\sqrt{2}c, & \alpha = 5,6,7,8 \end{cases} \tag{3}$$

where $c = \Delta x/\Delta t$, and Δx is the lattice spacing (In this paper, we choose $\Delta x = \Delta t = 1$).
For the $D2Q9$ model, the equilibrium distribution function is expressed as:

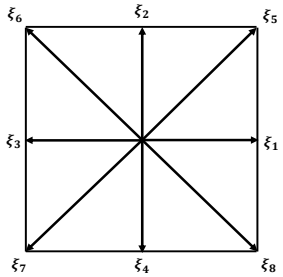

Figure 1: Discrete velocities of the $D2Q9$ model

$$f_\alpha^{eq}(\boldsymbol{x},t) = w_\alpha\rho\left[1 + \frac{\boldsymbol{\xi}_\alpha\cdot\boldsymbol{u}}{c_s^2} + \frac{\boldsymbol{uu}:(\boldsymbol{\xi}_\alpha\boldsymbol{\xi}_\alpha - c_s^2 I)}{2c_s^4}\right] \tag{4}$$

where w_α is the weighting factor given by:

$$w_\alpha = \begin{cases} 4/9, & \alpha = 0 \\ 1/9, & \alpha = 1,2,3,4 \\ 1/36, & \alpha = 5,6,7,8 \end{cases} \tag{5}$$

c_s is the speed of sound ($c_s = c/\sqrt{3}$ for the $D2Q9$ model) and I is the identity matrix. The incompressible Navier-Stokes equations (1) can be obtained from equation (2), using the Chapman-Enskog procedure. This procedure leads to the following expression for the kinematic viscosity of the fluid:

$$\nu = c_s^2 \Delta t(\tau - \frac{1}{2}) \tag{6}$$

In the lattice Boltzmann equation, the forcing term F_α, that represents the body force term $\boldsymbol{f}$ in the Navier-Stokes equations, was modeled using the formulation proposed by Guo et al. [44]:

$$F_\alpha = \left(1 - \frac{1}{2\tau}\right) w_\alpha \left[\frac{\boldsymbol{\xi}_\alpha - \boldsymbol{u}}{c_s^2} + \frac{(\boldsymbol{\xi}_\alpha \cdot \boldsymbol{u})}{c_s^4}\boldsymbol{\xi}_\alpha\right] \cdot \boldsymbol{f} \tag{7}$$

where the macroscopic quantities are calculated as follows:

$$\rho = \sum_\alpha f_\alpha(\boldsymbol{x}, t) \tag{8}$$

$$\rho \boldsymbol{u} = \sum_\alpha \boldsymbol{\xi}_\alpha f_\alpha(\boldsymbol{x}, t) + \frac{\Delta t}{2}\boldsymbol{f} \tag{9}$$

As demonstrated by Guo et al., this force treatment leads to the exact Navier-Stokes equations.

2.1.2. Multiple Relaxation Time LBM

This model, which was first introduced by d'Humières [45], is more stable than the single relaxation time lattice Boltzmann model. With this model, the collision process is carried out in the moment space. A transformation matrix M enables to express the moments $m_\alpha(\boldsymbol{x}, t)$ according to the distribution functions $f_\alpha(\boldsymbol{x}, t)$. The lattice Boltzmann equation with a source term, as given by Lu et al. [46], becomes:

$$\begin{aligned} |f_\alpha(\boldsymbol{x} + \boldsymbol{\xi}_\alpha \Delta t, t + \Delta t)\rangle - |f_\alpha(\boldsymbol{x}, t)\rangle = \\ - M^{-1}[S(|m_\alpha(\boldsymbol{x}, t)\rangle - |m_\alpha^{eq}(\boldsymbol{x}, t)\rangle) - (I - S/2)M\Delta t|F_\alpha(\boldsymbol{x}, t)\rangle] \end{aligned} \tag{10}$$

In this equation, $|\bullet\rangle$ denotes a column vector and I is the identity matrix. The moments $|m_\alpha(\boldsymbol{x}, t)\rangle = (m_0, m_1, \ldots, m_8)^T$ are deduced from:

$$|m_\alpha(\boldsymbol{x}, t)\rangle = M|f_\alpha(\boldsymbol{x}, t)\rangle \Rightarrow |f_\alpha(\boldsymbol{x}, t)\rangle = M^{-1}|m_\alpha(\boldsymbol{x}, t)\rangle \tag{11}$$

The corresponding equilibria of the moments are given by:

$$|m_\alpha^{eq}(\boldsymbol{x}, t)\rangle = \rho(1, -2 + 3(u^2 + v^2), 1 - 3(u^2 + v^2), u, -u, v, -v, u^2 - v^2, uv)^T \tag{12}$$

The transformation matrix M is:

$$M = \begin{pmatrix} 1 & 1 & 1 & 1 & 1 & 1 & 1 & 1 & 1 \\ -4 & -1 & -1 & -1 & -1 & 2 & 2 & 2 & 2 \\ 4 & -2 & -2 & -2 & -2 & 1 & 1 & 1 & 1 \\ 0 & 1 & 0 & -1 & 0 & 1 & -1 & -1 & 1 \\ 0 & -2 & 0 & 2 & 0 & 1 & -1 & -1 & 1 \\ 0 & 0 & 1 & 0 & -1 & 1 & 1 & -1 & -1 \\ 0 & 0 & -2 & 0 & 2 & 1 & 1 & -1 & -1 \\ 0 & 1 & -1 & 1 & -1 & 0 & 0 & 0 & 0 \\ 0 & 0 & 0 & 0 & 0 & 1 & -1 & 1 & -1 \end{pmatrix} \tag{13}$$

S is a diagonal matrix that contains the relaxation rates of each moment:

$$S = diag(s_0, s_1, s_2, s_3, s_4, s_5, s_6, s_7, s_8) = diag(0, s_n, s_n, 0, s_q, 0, s_q, s_n, s_n) \tag{14}$$

Ginzburg and d'Humières [8] showed that, for straight boundaries, the numerical slip at the fluid-solid interface can be avoided if the following relationship is satisfied:

$$\Lambda = \left(\frac{1}{s_n} - \frac{1}{2}\right)\left(\frac{1}{s_q} - \frac{1}{2}\right) \tag{15}$$

with $\Lambda = \dfrac{3}{16}$ and $s_n = \dfrac{1}{\tau}$. The last term in equation (10) represents the forcing term developed by Lu et al. [46] for the MRT LBM, which is a general formulation of the forcing term proposed by Guo et al. [44] for the SRT LBM. In this expression, F_α is calculated according to:

$$F_\alpha = w_\alpha \left(\frac{\boldsymbol{\xi}_\alpha - \boldsymbol{u}}{c_s^2} + \frac{(\boldsymbol{\xi}_\alpha \cdot \boldsymbol{u})}{c_s^4}\boldsymbol{\xi}_\alpha\right) \cdot \boldsymbol{f} \tag{16}$$

When all relaxation rates are equal to $\dfrac{1}{\tau}$, the MRT model leads to the SRT model, including the forcing term developed by Guo et al. [44].

2.2. Volume penalization method

The aim of this work is to apply the volume penalization method in a lattice Boltzmann framework to take into account the presence of an obstacle in a flow. In the volume penalization method, the body force term in the Navier-Stokes equations (1) applies to all Cartesian nodes of the whole computational domain (fluid domain and solid domain). The volume source term reads:

$$\boldsymbol{f} = -\rho\frac{\chi}{\eta}(\boldsymbol{u} - \boldsymbol{u}_s) \tag{17}$$

where χ is a mask function equal to 0 in the fluid domain, and 1 in the solid domain, η is a permeability or penalization parameter, that is very small (for all computations, a value of $\eta = 10^{-7}$ was chosen), and $\boldsymbol{u}_s$ is the solid velocity. With this method, the penalization term is very high in the solid domain, hence the velocity is equal to the solid velocity, and it is null in the fluid domain. This penalization term is introduced into the lattice Boltzmann equation (2) (SRT lattice Boltzmann equation) or (10) (MRT lattice Boltzmann equation),

using the forcing term proposed by Guo et al. (7) (for the SRT LBM) or (16) (for the MRT LBM). The lattice Boltzmann equation is solved on both fluid and solid domains. Equation (9) is used to calculate the velocity in the fluid and solid domains. The right hand side of this equation contains the fluid velocity via the penalization term $\boldsymbol{f}$. This leads to the following expression for the velocity:

$$\boldsymbol{u} = \frac{\sum_{\alpha} \boldsymbol{\xi_\alpha} f_\alpha + \frac{\Delta t}{2}\frac{\chi}{\eta}\rho \boldsymbol{u_s}}{\rho + \frac{\Delta t}{2}\frac{\chi}{\eta}\rho} \tag{18}$$

Since the velocity boundary condition is naturally applied at the solid obstacle thanks to the mask function, this method is easy to implement.

3. Numerical results and discussion

In this section, we present numerical results obtained with the VP-LBM. In a first step, the VP LBM approach was evaluated by simulating flows for which an analytical solution is known: a symmetric shear flow between two moving plates, and a Couette flow between two cylinders. These test cases were chosen by Le and Zhang [47] and by Lu et al. [46] for evaluating the immersed boundary approach combined with the lattice Boltzmann method. Our results will therefore also be compared with the results computed by Lu et al. with the IB-LBM (Immersed Boundary Lattice Boltzmann Method). In a second step, more complex flows were treated: flow past a cylinder at a Reynolds number of 500, and flow induced vibration of a cylinder at a Reynolds number of 100. It will be showed that all these tested cases yielded satisfactory results.

3.1. Symmetric shear flow

First, we focused on a symmetric shear flow, between two moving parallel plates (see figure 2) with a thickness $e = 50\ l.u.$

This configuration was modeled by Le and Zhang [47], Lu et al. [46], and Farnoush and

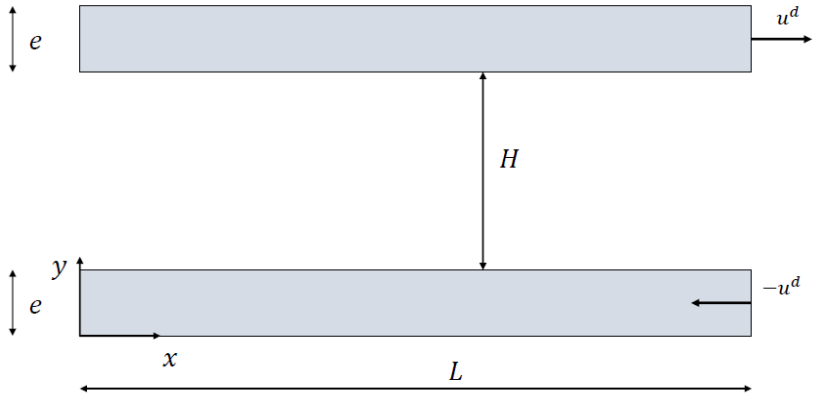

Figure 2: The symmetric shear flow case

Manzari [48], who analyzed the immersed boundary method combined with the lattice Boltzmann method. The length of the domain is $L = 200\ l.u.$, and the distance between the two plates is $H = 100\ l.u$. The upper and lower plates move according to x direction, with velocities u^d and $-u^d$, respectively. Periodic boundary conditions were applied according to x and y directions. For this configuration, the lattice Boltzmann simulations were performed with a maximum lattice velocity that ensured that the Mach number was small ($u^d = 0.01\ l.u.$). For this steady unidirectional flow in the absence of a pressure gradient, the analytical solution of the Navier-Stokes equations is:

$$u_{analytical}(y) = \frac{2u^d}{H}(y - e) - u^d \tag{19}$$

The relative L_2 error of u in the fluid domain was calculated according to:

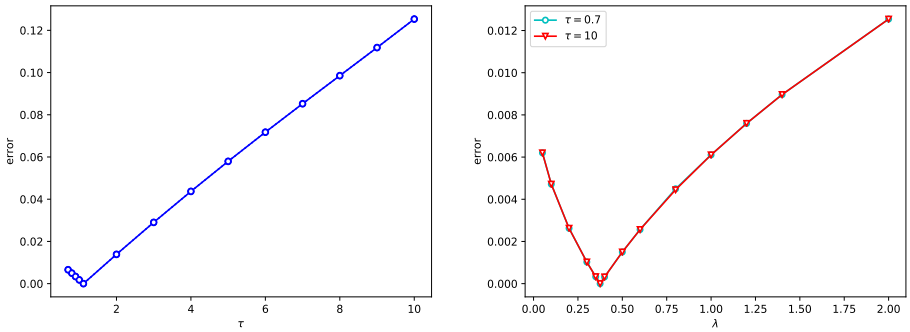

(a) influence of τ (VP SRT LBM) (b) influence of Λ (VP MRT LBM)

Figure 3: (a) Influence of τ on the relative L_2 error of u, for the symmetric shear flow (VP SRT LBM); (b) Influence of Λ on the relative L_2 error of u, for the symmetric shear flow (VP MRT LBM).

$$error = \frac{\sqrt{\sum (u - u_{analytical})^2}}{\sqrt{\sum (u_{analytical})^2}} \tag{20}$$

where the summation was performed in the fluid domain, and u and $u_{analytical}$ are respectively the computed horizontal velocity and the analytical solution. Figure 3 compares the relative L_2 error of u in the fluid domain, computed when using the volume penalization method and the single relaxation time lattice Boltzmann method (VP SRT) on the one hand, and the multiple relaxation time lattice Boltzmann method (VP MRT) on the other hand. In this figure, we can see that the error was very close to zero for $\tau = \frac{1}{2} + \frac{\sqrt{6}}{4} \approx 1.11$ when the flow was computed with the single relaxation time LBM, and for $\Lambda = \frac{3}{8} = 0.375$ when the multiple relaxation time LBM was applied.

In figure 4 , the difference between the exact solution and the numerical results obtained with the SRT LBM (figure (a)) and the MRT LBM (figure (c)), and the corresponding velocity profiles at $x = L/2$ (figure (b) for the SRT LBM and figure (d) for the MRT LBM with

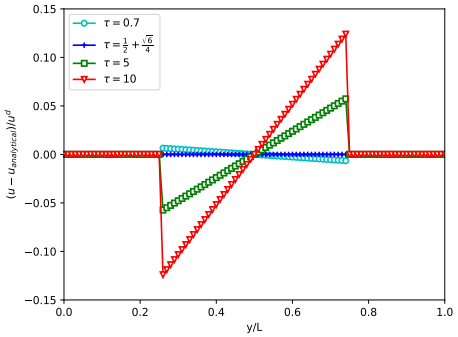

(a) difference between the numerical (VP SRT LBM) and the exact horizontal velocities

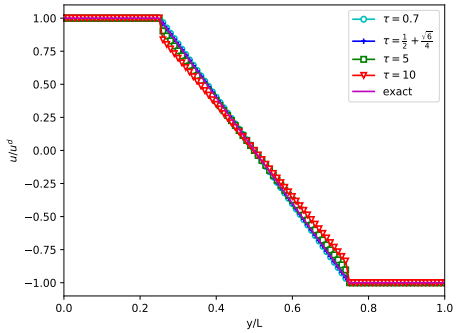

(b) horizontal velocity obtained with the VP SRT LBM

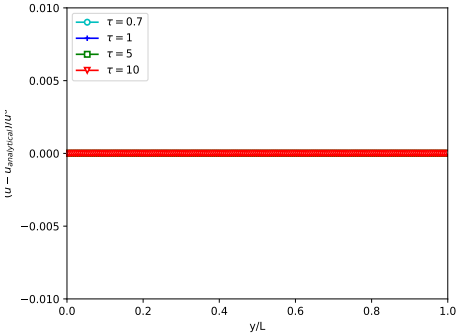

(c) difference between the numerical (VP MRT LBM) and the exact horizontal velocities

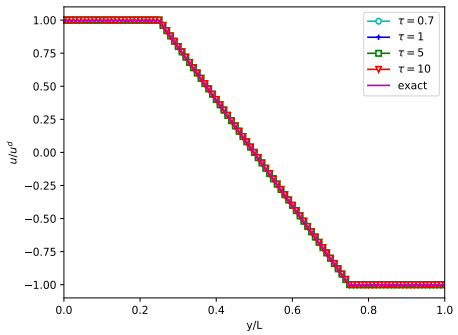

(d) horizontal velocity obtained with the VP MRT LBM

Figure 4: Difference between the numerical and the exact velocities (a) and (c), and velocity profiles (b) and (d), obtained at $x = L/2$, for the symmetric shear flow. For the VP MRT LBM computations, $\Lambda = \frac{3}{8}$ was used.

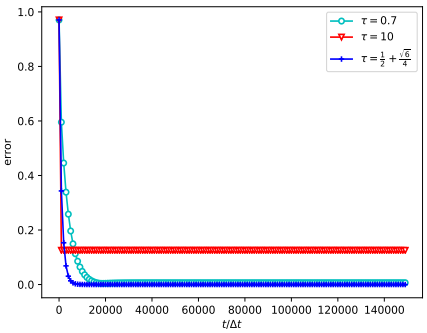

Figure 5: Convergence history of the VP SRT LBM, for the symmetric shear flow case.

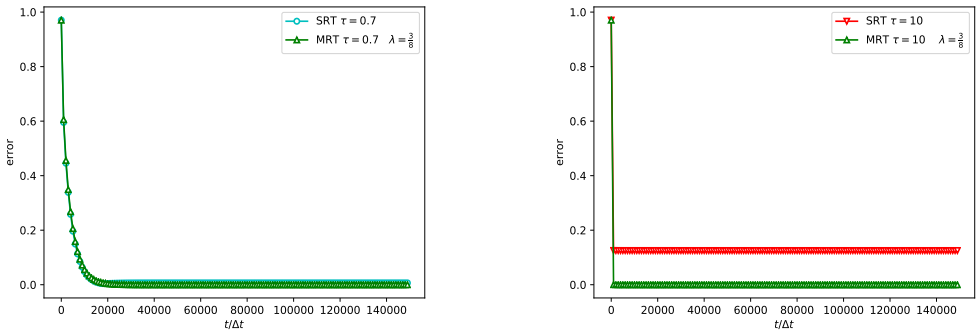

(a) $\tau = 0.7$ (b) $\tau = 10$

Figure 6: Convergence history of the VP MRT LBM for the symmetric shear flow case ($\tau = 0.7$ and $\tau = 10$).

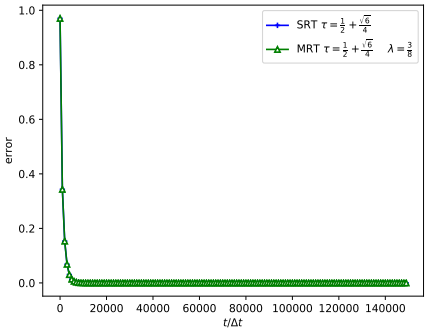

Figure 7: Convergence histories of the VP SRT LBM ($\tau = \frac{1}{2} + \frac{\sqrt{6}}{4}$), and of the VP MRT LBM ($\tau = \frac{1}{2} + \frac{\sqrt{6}}{4}$, $\Lambda = \frac{3}{8}$), for the symmetric shear flow case.

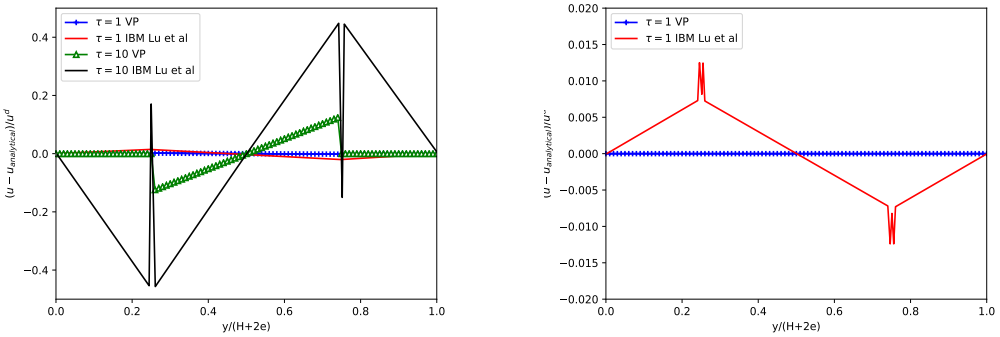

(a) SRT LBM (b) MRT LBM

Figure 8: Comparison of the errors obtained with the volume penalization LBM, with those obtained with an immersed boundary LBM by Lu et al. [46], for the symmetric shear flow case.

$\Lambda = \frac{3}{8}$) are presented. We can see that the velocity calculated in the solid domain is the solid velocity naturally applied thanks to the penalization technique. For the Multiple Relaxation Time LBM with $\Lambda = \frac{3}{8}$, the solution is very close to the exact solution for all relaxation times.

Figures 5 , 6 , and 7 show that converged results with an error very close to zero were obtained with the smallest number of iterations when using the VP SRT LBM with $\tau = \frac{1}{2}+\frac{\sqrt{6}}{4}$ or the VP MRT LBM with $\tau = \frac{1}{2} + \frac{\sqrt{6}}{4}$ and $\Lambda = \frac{3}{8}$. In figure 7 , we can also remark that using the VP SRT LBM with $\tau = \frac{1}{2} + \frac{\sqrt{6}}{4}$ or the VP MRT LBM with $\Lambda = \frac{3}{8}$ leads to the same error, which is very close to zero. Indeed, for the SRT LBM, we have: $s_n = s_q = \frac{1}{\tau}$, this implies: $\Lambda = (\tau - \frac{1}{2})^2 = \frac{3}{8}$, and thus: $\tau = \frac{1}{2} + \frac{\sqrt{6}}{4}$. Furthermore, as mentioned previously, Ginzburg and d'Humières [8] showed that, when applying the half way bounce back boundary condition, exact solutions can be obtained for Poiseuille and Couette flows, if $\Lambda = \frac{3}{16}$. Lu et al. [46], who conducted a theoretical analysis on the Immersed Boundary Lattice Boltzmann Method, showed that, for similar flow cases, the error can be decreased but not eliminated for $\Lambda = \frac{9}{8}$.
For this case, we also compared the results given by the volume penalization method, with those obtained with the immersed boundary method by Lu et al. [46] on the same grid (see figure 8). In this case involving straight boundaries, it can be noticed that for high relaxation times, the immersed boundary method combined with the single relaxation time LBM results in a higher error as compared with the results obtained with the volume penalization method (figure 8 (a)). We can also remark that while the error is very close to zero when using the volume penalization method together with the multiple relaxation time LBM, it cannot be eliminated when implementing the immersed boundary method in a multiple relaxation time LBM (figure 8 (b)).

3.2. Flow between two cylinders

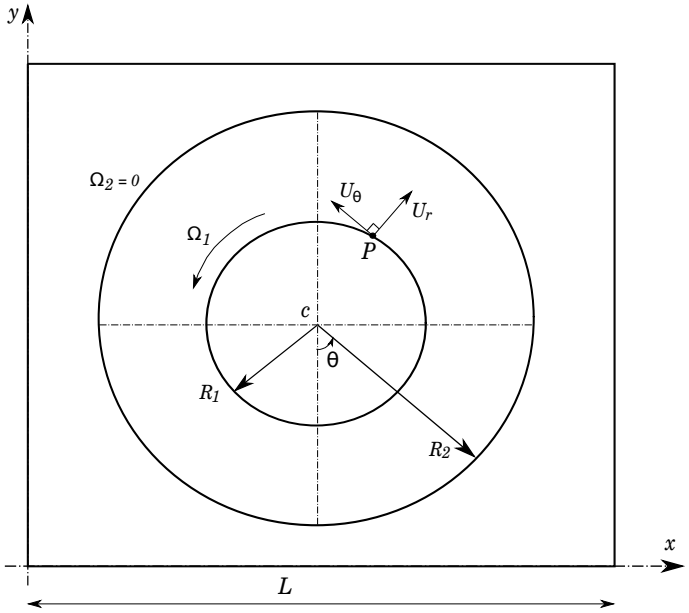

Figure 9: The cylindrical Couette flow case.

In this part of the study, we applied the VP LBM to a curved boundary, by focusing on a flow between two cylinders, as shown in figure 9 . The length and width of the square computational domain are $L = 200\ l.u.$, and the radii of the inner and the outer cylinders located in the center of the domain, are $R_1 = 45\ l.u.$ and $R_2 = 70\ l.u.$ respectively. While the outer cylinder is motionless ($\Omega_2 = 0$), the inner cylinder moves according to the angular velocity $\Omega_1 = u^d/R_1$. In the computations, u^d was small enough to deal with a low Mach number flow ($u^d = 0.01\ l.u.$). This configuration was studied by [47] and [46], who evaluated the immersed boundary method implemented in a lattice Boltzmann framework. For this case, the analytical profile of the tangential velocity component is:

$$U_{\theta\ analytical} = \frac{-u^d R_1}{(R_2^2 - R_1^2)}\, r + \frac{u^d R_1 R_2^2}{(R_2^2 - R_1^2)}\, \frac{1}{r} \tag{21}$$

where r is the cylindrical coordinate.

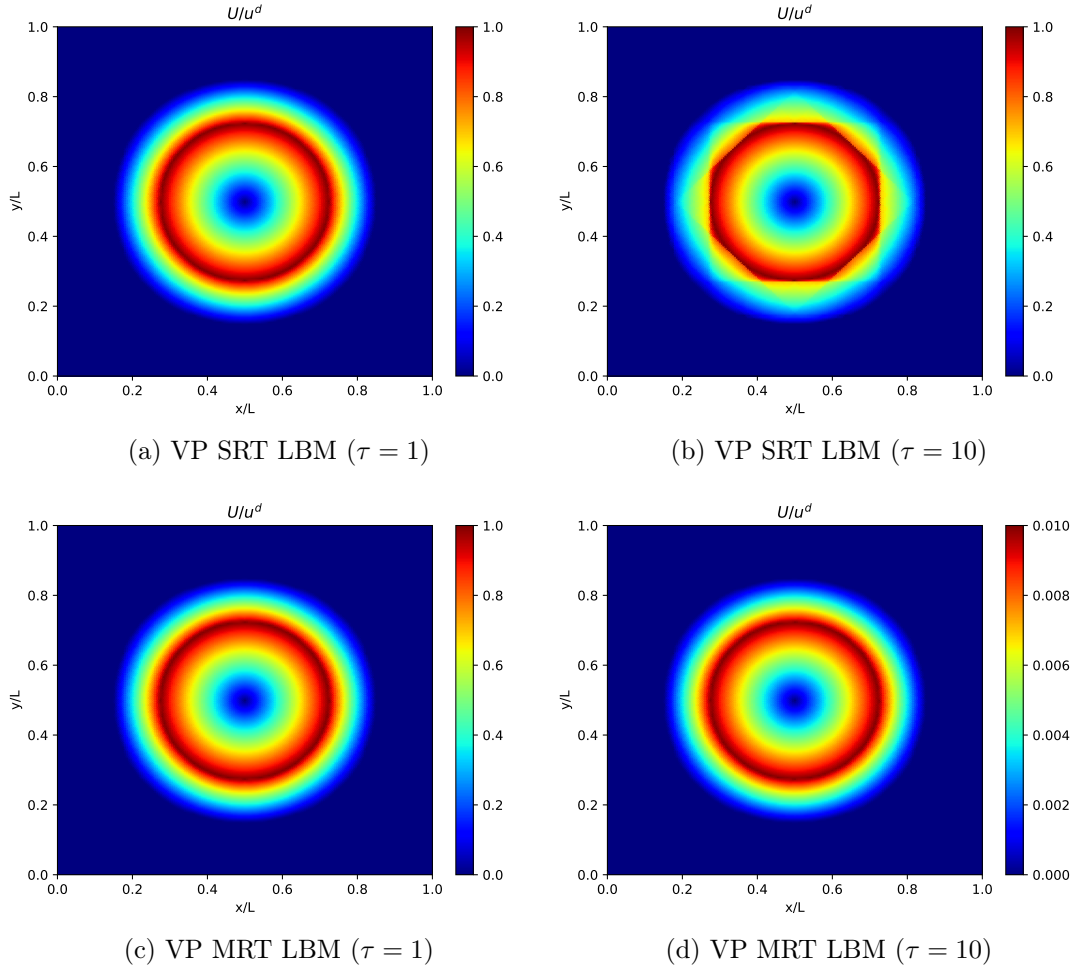

(a) VP SRT LBM ($\tau = 1$)

(b) VP SRT LBM ($\tau = 10$)

(c) VP MRT LBM ($\tau = 1$)

(d) VP MRT LBM ($\tau = 10$)

Figure 10: Isocontours of velocity magnitude obtained for the cylinder case.

Figure 10 displays the isovalues of the velocity magnitude computed with the single relaxation time LBM and the multiple relaxation time LBM, for two relaxation times ($\tau = 1$ and $\tau = 10$). In this figure, we can see that unrealistic results are obtained if a high relaxation time is chosen when the flow is computed with the single relaxation time LBM ($\tau = 10$, figure 10 (b)). This problem does not occur when the multiple relaxation time model is applied (see figure 10 (d)).

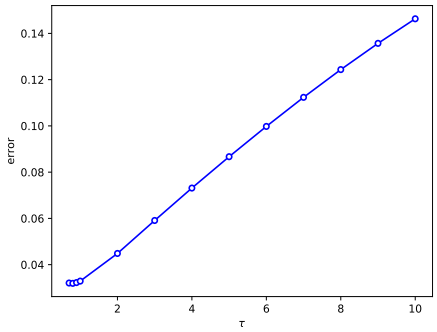

Figure 11: Influence of τ on the relative L_2 error of v, for the flow between two cylinders (VP SRT LBM).

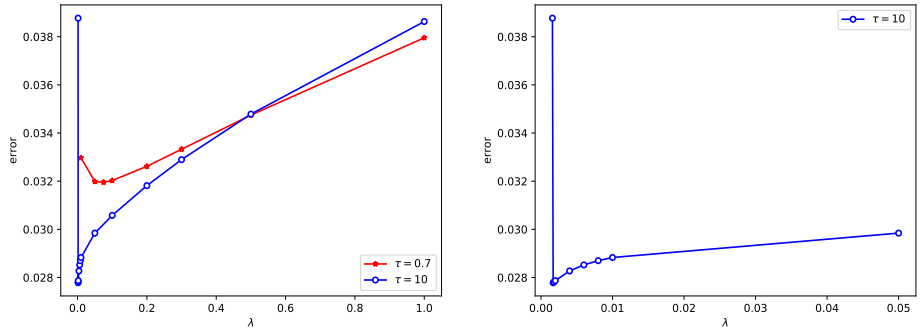

(a) influence of Λ (VP MRT LBM) (b) influence of Λ for $\tau = 10$: zoom on $\Lambda < 0.06$

Figure 12: (a) and (b) Influence of Λ on the relative L_2 error of v, for the flow between two cylinders (VP MRT LBM).

In figure 11 , the relative L_2 error of v in the fluid domain as a function of the relaxation time, computed with the single relaxation time LBM, is plotted. In contrast with the previous cases which involved straight boundaries, this case deals with a curved boundary which is approximated in a staircase manner; this induces an error for all τ values. A similar remark can be done when examining the evolution of the relative L_2 error of v according to Λ, for the computations performed with the multiple relaxation time LBM (see figure 12 (a)) and a relaxation time $\tau = 0.7$. For a higher relaxation time ($\tau = 10$), the optimal value of Λ that

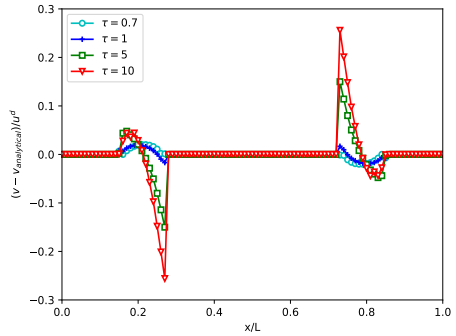

(a) difference between the numerical (VP SRT LBM) and the exact vertical velocities

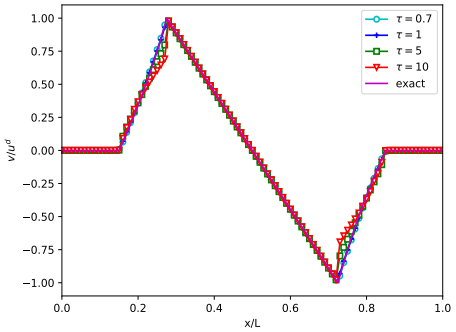

(b) vertical velocity obtained with the VP SRT LBM

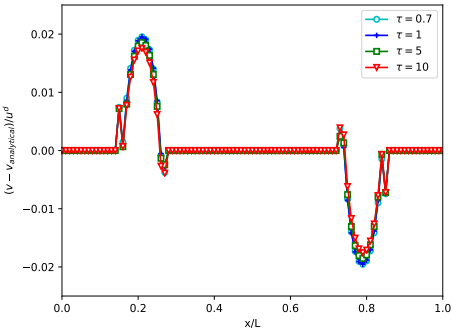

(c) difference between the numerical (VP MRT LBM) and the exact vertical velocities

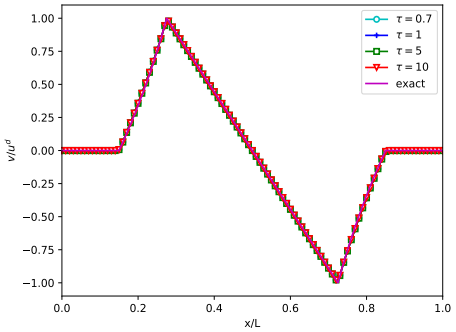

(d) vertical velocity obtained with the VP MRT LBM

Figure 13: Difference between the numerical and the exact velocities, and velocity profiles, obtained at $y = L/2$, for the cylinder case.

minimizes the error is closer to zero, and the error is smaller than for $\tau = 0.7$ (see figures 12 (a) and (b)).

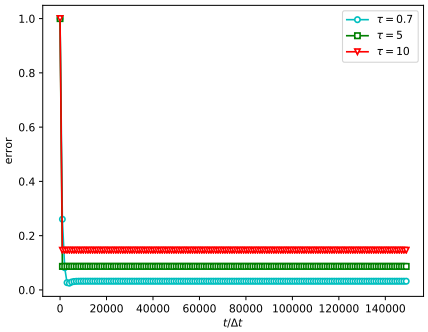

Figure 14: Convergence history of the VP SRT LBM, for the cylinder case.

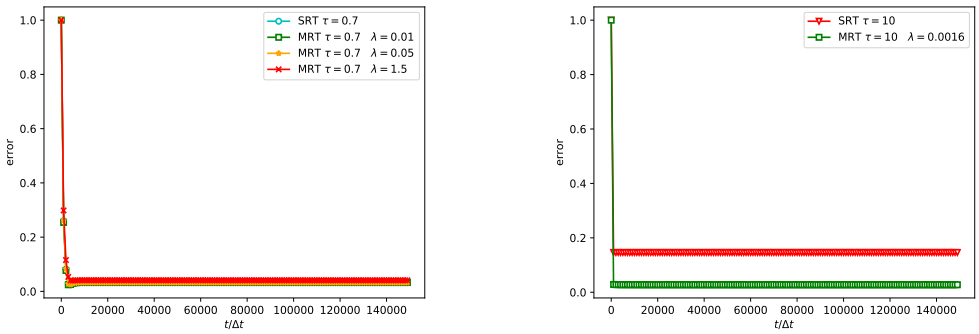

(a) $\tau = 0.7$ (b) $\tau = 10$

Figure 15: Convergence history of the VP MRT LBM, for the cylinder case.

Figures 13 (a) and (c) show the profiles of the difference (made non dimensional with u^d) between the numerical and the exact solutions, obtained with the single relaxation time LBM, and with the multiple relaxation time LBM, at $y = L/2$. The corresponding velocity profiles are plotted in figures 13 (b) and (d). The optimal values of Λ that minimize the relative L_2 error of v were used for the computations performed with the MRT LBM. In this figure, we notice that, for high values of the relaxation time, the volume penalization MRT model produces errors that are smaller than the ones obtained with the volume penalization SRT model. High differences can also be seen at the fluid-solid interface for the VP SRT LBM and high values of the relaxation time. For this case with curved boundaries, we can also remark that when applying the MRT LBM with $\tau = 10$ and $\Lambda = 0.0016$, converged results are obtained after a smaller number of iterations than with other relaxation times (for the MRT LBM, and the SRT LBM, see figures 14 and 15). However, the discrepancy between $\tau = 0.7$ and $\tau = 10$ for the MRT LBM is not high.

In figure 16 , we also compared the errors obtained with the volume penalization LBM (SRT and MRT) with those computed with the immersed boundary method (and the same grid) by Lu et al. [46]. In this figure, we can notice that the error in the vicinity of the solid boundary is higher with the volume penalization method that approximates the curved boundary with a staircase manner, than with the immersed boundary method that takes the curved shape of the boundary into consideration. The error in the rest of the fluid domain is lower when the flow is predicted with the VP LBM.

For this case, we also studied the influence of the grid on the accuracy of the results. To do that, we carried out simulations with the multiple relaxation time LBM, and for a relaxation time $\tau = 0.7$. The number of cells according to the x and y directions was varied between 200 $l.u.$ and 800 $l.u.$ For the dense grid (800 $l.u.$), two cases were considered: one case where the number of grids Ngrid in the flow domain, according to x and y, was: $R_2 - R_1 = 100$ $l.u.$, and another case where this number was higher: $R_2 - R_1 = 125$ $l.u.$ (see table 1). In figure 17 , the evolution of the relative L_2 error of v according to the parameter Λ is presented. We can see that for a higher number of cells in the flow domain, the error

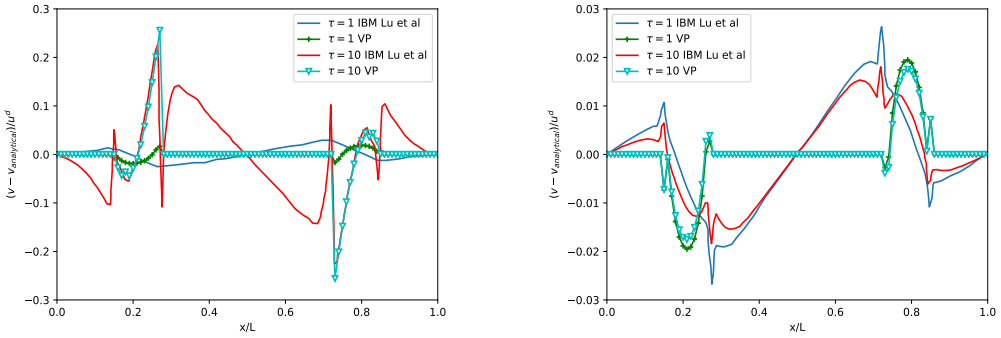

(a) SRT LBM (b) MRT LBM

Figure 16: Comparison of the errors obtained with the volume penalization LBM, with those computed with an immersed boundary LBM by Lu et al. [46], for the cylinder case.

decreases and the results are less dependent on the parameter Λ. To accurately describe the curved surface with the volume penalization method, a large number of grids must thus be used.

L $(l.u.)$	Ngrid $(l.u.)$
200	25
400	50
600	75
800	100
800	125

Table 1: Grid resolutions tested for the cylinder case

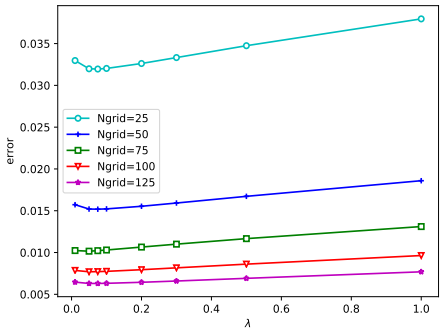

Figure 17: Influence of the grid resolution on the relative L_2 error of v, for the flow between two cylinders (VP MRT LBM, $\tau = 0.7$).

3.3. Flow past a circular cylinder at a Reynolds number of 500

The cases presented in the previous paragraphs deal with low Reynolds number flows. In our previous paper, we applied the VP LBM method to the computation of the flow past a cylinder at a Reynolds number of 100. In this paper, to evaluate the ability of the VP LBM to handle more complex flows, we focused on the flow around a circular cylinder at a Reynolds number of 500 (the Reynolds number is based on the diameter D of the cylinder and the free stream velocity U_0). The computational domain is presented in figure 18 . For that case, the boundary conditions at the upper and lower horizontal planes were symmetry boundary conditions, a constant velocity profile was applied at the inlet, and a convective condition, as proposed by Yang [49], was employed for the outlet. The dimensions of the domain are $30D$ in the horizontal direction, $10D$ in the vertical direction, and the distance between the cylinder and the outlet is equal to $25D$.

As highlighted in the previous paragraph, a large number of grids must be used to describe properly a curved surface, when using the volume penalization method. Hence, the domain was discretized with 6048 lattices according to the horizontal direction, 2016 lattices according to the vertical direction, and 201 lattices along the diameter of the cylinder. A velocity of 0.05 was imposed at the inlet. For that case which involved a large number of grids, the VP-LBM code was parallelized with CUDA. The computations were carried out with Graphics Processing Units (GPUs), and the multiple relaxation time lattice Boltzmann method was used. A non dimensional relaxation time $\tau = 0.56$ was chosen.

In figure 19 which displays the instantaneous isovalues of velocity magnitude around the cylinder, we can see the vortex shedding phenomenon that occurs behind the cylinder. With the momentum exchange method proposed by Wen et al. [50], the drag force F_D and the lift force F_L exerted on the cylinder were calculated, and the drag and lift coefficients C_D and C_L were obtained from the following relationships:

$$C_D = \frac{F_D}{\frac{1}{2}\rho U_0^2 D} \text{ and } C_L = \frac{F_L}{\frac{1}{2}\rho U_0^2 D} \tag{22}$$

The Strouhal number was also calculated as follows:

$$St = \frac{fD}{U_0} \tag{23}$$

where f is the frequency of the vortex shedding. In figure 20 , where the evolutions of the drag and the lift coefficients according to the non dimensional time are presented, a periodic behavior of these coefficients can be noticed. The average drag coefficient C_{Dave}, the root mean square of the lift coefficient C_{Lrms}, and the Strouhal number were compared with experimental results found in the literature [51, 52], and with numerical results obtained with the finite volume method (FVM), and more particularly with the OpenFOAM [53] code, on a structured mesh. In table 2, we can see that the results calculated with the VP-LBM are in a satisfactory agreement with experimental results, and with numerical results computed with the finite volume method.

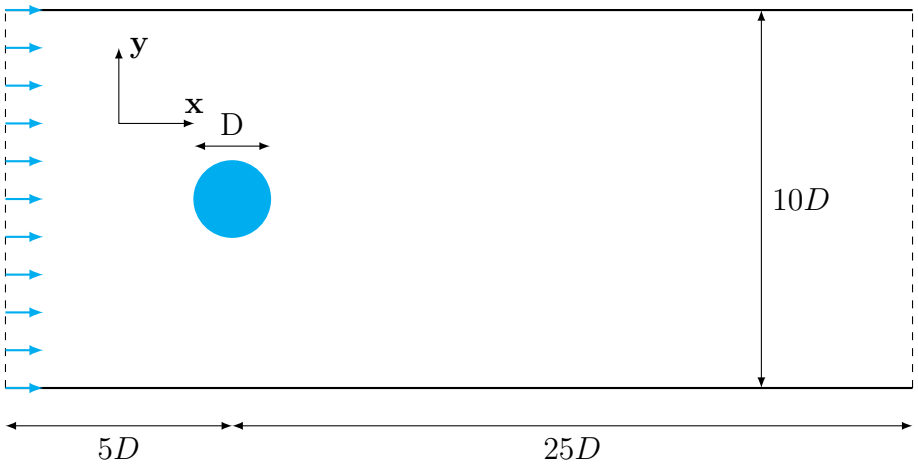

Figure 18: Computational domain for the flow around a cylinder

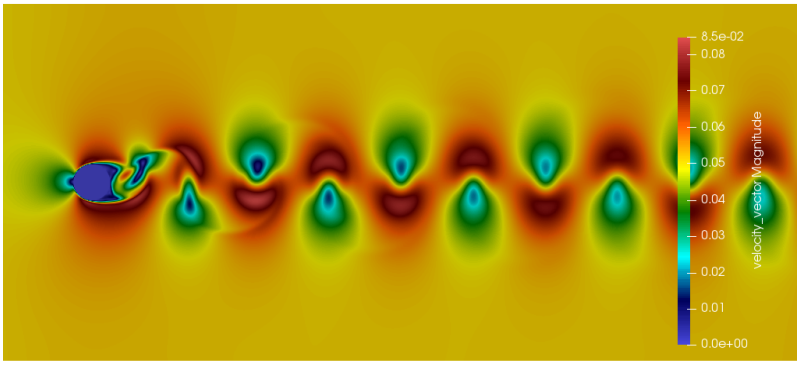

Figure 19: Instantaneous isovalues of velocity magnitude behind the cylinder ($Re = 500$).

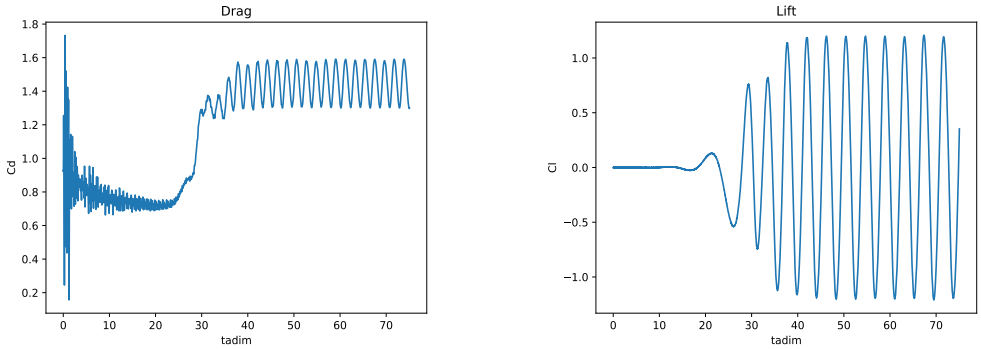

(a) Drag coefficient

(b) Lift coefficient

Figure 20: Drag and lift coefficients obtained with the VP LBM, for the flow past a circular cylinder, at a Reynolds number of 500.

3.4. Flow induced vibration of a cylinder at a Reynolds number of 100

To finish with, the flow induced vibration of a cylinder at a Reynolds number of 100 was calculated with the VP-LBM approach. For that fluid structure interaction case, the

	VP-LBM	FVM	Experiments
C_{Dave}	1.45	1.43	1.45 [52]
C_{Lrms}	0.84	0.82	
St	0.22	0.22	0.21 [51]

Table 2: Results obtained for a flow around a cylinder at a Reynolds number of 500

computations were performed with the VP-LBM code parallelized with CUDA, and also with the CPU version of the VP-LBM code. The boundary conditions applied on the fluid domain were the same as in the previous paragraph (see figure 21) , but the cylinder, which was submitted to a force normal to the freestream, exerted by a spring, and to the fluid lift force, moved according to the following equation:

$$m\ddot{y}_G + k\left(y_G - y_0\right) = \mathcal{F}_y \tag{24}$$

where m is the cylinder mass, y_G is the position of the gravity center of the cylinder according to y, and y_0 is its position at rest, k is the spring constant and $\mathcal{F}_y$ is the lift force. To compare our results with those found in literature (Shiels et al. [54]), equation (24) was made non dimensional as follows:

$$m^*\ddot{y}^* + k^*\left(y^* - y_0^*\right) = C_L \tag{25}$$

with the non dimensional parameters:

$$m^* = \frac{m}{0.5\rho D^2} \quad k^* = \frac{k}{0.5\rho U_0^2} \quad y^* = \frac{y_G}{D} \quad C_L = \frac{\mathcal{F}_y}{\frac{1}{2}\rho U_0^2 D} \quad t^* = t\frac{U_0}{D}$$

To gather the results obtained with various parameters k^* and m^* on a unique plot, Shiels et al. [54] introduced the effective dimensionless stiffness:

$$k^*_{\text{eff}} = k^* - m^*\omega^{*2}, \tag{26}$$

where ω^* is the oscillating frequency of the cylinder (it is calculated with the results obtained from the computations).

Several computations were performed, with an increasing number of lattices in the cylinder. The parameters used for these computations are given in Table 3.

D	τ	U_0	L_1	L_2
41	0.56	0.0487	1230	410
81	0.6	0.0397	2430	810
209	0.75	0.0398	6270	2090

Table 3: Parameters used for computating the flow induced vibration of a cylinder

For the cylinder equation of motion, the non dimensional cylinder mass and spring constant were assigned the following values:

$$k^* = 21.724 \quad m^* = 10$$

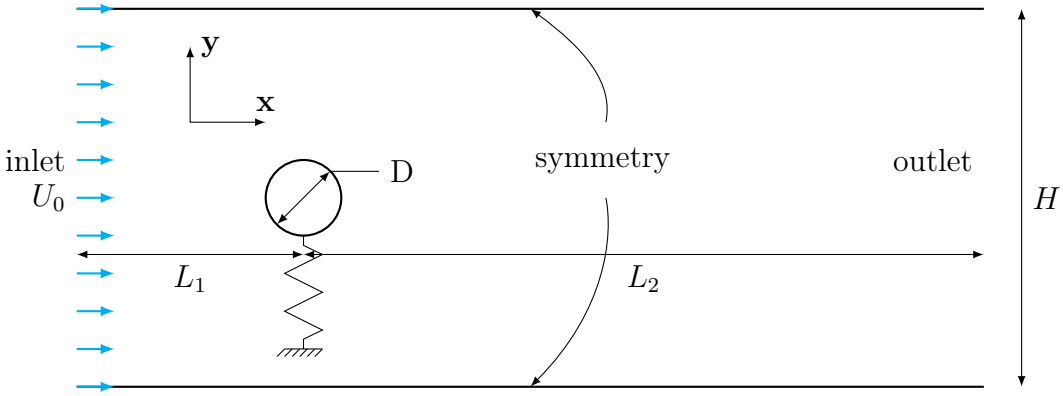

Figure 21: Computational domain for the flow induced vibration of a cylinder

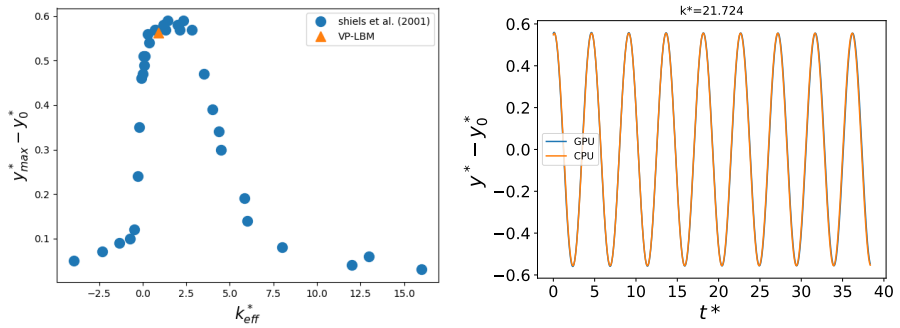

(a) Response of the system against the effective stiffness

(b) Cylinder response

Figure 22: Comparison of our results with those found in literature [54]

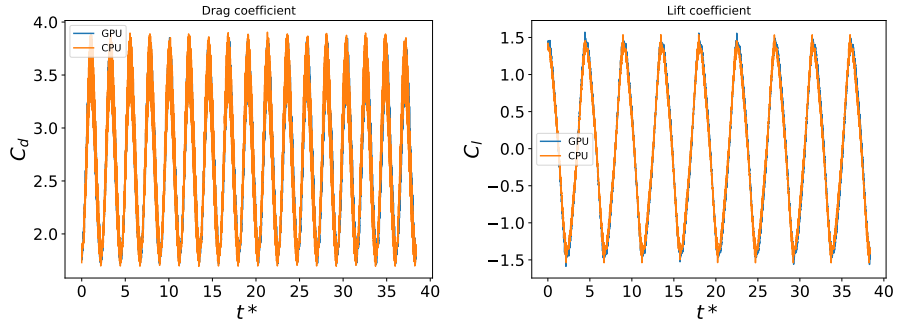

(a) Drag coefficient

(b) Lift coefficient

Figure 23: Temporal evolutions of the drag and lift coefficients

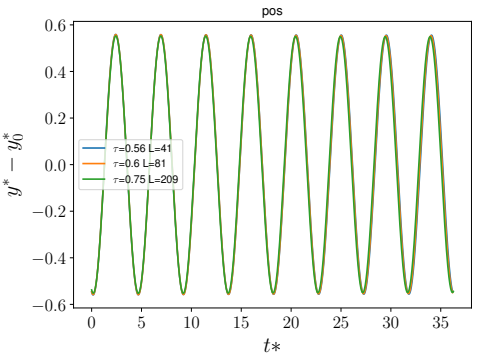

Figure 24: Cylinder response, for the three tested grids

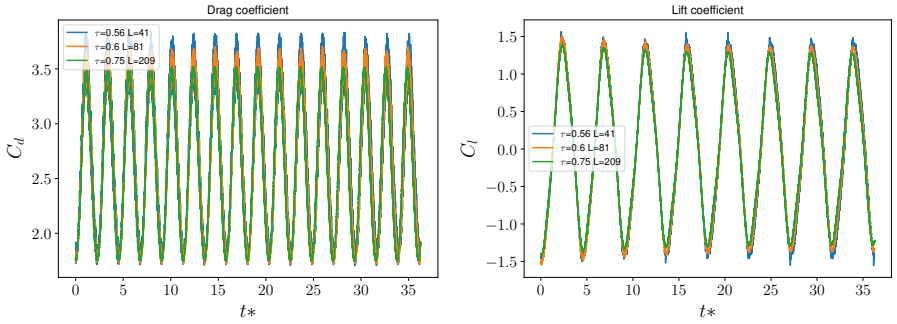

(a) Drag coefficient (b) Lift coefficient

Figure 25: Temporal evolutions of the drag and lift coefficients, for the three tested grids

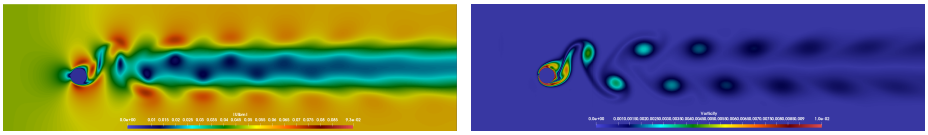

(a) Velocity field in lattice units (b) Vorticity field in lattice units

Figure 26: Velocity and vorticity fields obtained with the VP-LBM for the flow induced vibration of a cylinder at a Reynolds number of 100

Figures 22 and 23 show a comparison of the results obtained with the CPU and the GPU, with the smallest number of grids (41 cells through the diameter of the cylinder). In figure 22 (a), we can see that for the parameters selected for this computation, the cylinder oscillates with a large amplitude which is greater than 50% of the cylinder diameter, this corresponds to the lock-in behavior. The oscillation is periodic (see figure 22 (b)). In figure 23, the temporal evolutions of the drag coefficient and of the lift coefficient are plotted. The CPU code and the GPU code lead to similar results. In figures 24, 25(a), 25(b), the transverse motion of the cylinder, the oscillation of the drag force and of the lift force are plotted for the three tested grids. For the two coarsest grids, high frequency spurious oscillations of the

drag force and of the lift force can be noticed, which must be due to the volume penalization method, when the solid boundary 'jumps' from a cell to its neighbour. These oscillations disappear when the highest number of grids is used. It can also be seen in figure 24 that the cylinder motion is not sensitive to these force oscillations. Due to its inertia, the cylinder does not see these high frequency oscillations of the hydrodynamic forces, and the amplitude of the cylinder oscillation remains the same for the three tested grids. From the velocity field computed with the VP LBM, the vorticity field was obtained with Paraview software [55]. The effects of the cylinder oscillation on the downstream flow can be seen in figure 24 . The vortex shedding phenomenon is reduced, and the vortices gradually disappear in the wake of the cylinder.

4. Conclusions

In this paper, we presented a new approach for modeling fluid flows in the presence of solid obstacles. It consists in coupling the volume penalization method with the lattice Boltzmann approach. With this method, the lattice Boltzmann equation was applied on both solid and fluid media, and the solid domain was penalized in order to apply the solid velocity in the solid domain.

To evaluate this method, several cases were considered. First, the VP-LBM method was applied to cases for which an analytical solution is known: a symmetric shear flow, and a cylindrical Couette flow. The numerical results obtained with the volume penalization method combined with the Single Relaxation Time Lattice Boltzmann method on the one hand, and with the Multiple Relaxation Time Lattice Boltzmann method, on the other hand, were compared with the analytical solutions, and with results obtained by a combination of the immersed boundary method and the LBM, by Lu et al. [46] who performed a theoretical analysis of numerical slip velocity that occurs when using the immersed boundary LBM. For these cases, we noticed that the VP MRT lattice Boltzmann method enables to reduce the slip velocity in the solid domain, in comparison with the VP SRT LBM. For straight boundaries, this error was very close to zero when an optimum value of the relaxation time was used for the SRT LBM, and also when an optimum value of the parameter Λ was chosen for the MRT LBM. In the case with a curved boundary, the error could not be eliminated, but it was decreased when the MRT LBM was applied. Then, two complex unsteady flows were computed: a flow around a circular cylinder at a Reynolds number equal to 500, and the flow induced vibration of a cylinder at a Reynolds number of 100. To treat these cases, the Multiple Relaxation Time Lattice Boltzmann Method was chosen, the VP LBM code was parallelized with CUDA, and the computations were performed on Graphics Processing Units. A comparison of the results obtained for these cases, with results found in the literature was done, and a good agreement was highlighted.

To conclude with the VP-LBM, it can be noticed that it is physically meaningful, and easy to implement. Indeed, the computational domain where the Navier-Stokes equations (and thus the Lattice Boltzmann equation) are solved consists of the fluid and the solid media, and the volume force that is introduced into the Navier-Stokes equations, is applied on the whole solid domain thanks to a mask function, and it considers the obstacle as a porous

medium. In addition, the convergence of the volume penalization method has been mathematically proved [37]. In the context of the Lattice Boltzmann method, many researchers apply the immersed boundary method. The immersed boundary method consists in applying in the Navier-Stokes equations a volume force located on the surface of the obstacle and in spreading forces on the lattice nodes near the interface. With this method, the surface of the obstacle must be tracked during the computation, and it is less easy to implement this method in a highly parallelizable method such as the LBM. Even if the surface of the obstacle is modeled in a staircase manner with the volume penalization method, it enables to calculate flows around complex boundaries, and coupling this method with LBM makes the VP LBM an efficient parallel computing tool.

References

[1] J. Tolke, M. Krafczyk, TeraFLOP computing on a desktop PC with GPUs for 3D CFD, Int. J. Comput. Fluid D. 22(7) (2008) 443–456. doi:doi:10.1016/j.camwa.2010.03.057.

[2] C. Obrecht, F. Kuznik, B. Tourancheau, J. J. Roux, Multi-GPU implementation of the lattice Boltzmann method, Comput. Math. Appl. 65 (2013) 252–261. doi:doi:10.1016/j.camwa.2011.02.020.

[3] S. Chen, G. D. Doolen, Lattice Boltzmann method for fluid flows, Annu. Rev. Fluid Mech. 30 (1) (1998) 329–364. doi:10.1146/annurev.fluid.30.1.329.

[4] Z. Guo, C. Shu, Lattice Boltzmann method and its applications in engineering, World Scientific, 2013. doi:10.1142/8806.

[5] A. Ladd, Numerical simulations of particulate suspensions via a discretized Boltzmann equation. Part 1. Theoretical foundation, J. Fluid Mech. 271 (1994) 285–309. doi:10.1017/S0022112094001771.

[6] M. Bouzidi, M. Firdaouss, P. Lallemand, Momentum transfer of a Boltzmann-lattice fluid with boundaries, Phys. Fluids 13 (11) (2001) 3452–3459. doi:10.1063/1.1399290.

[7] D. Yu, R. Mei, L. Luo, W. Shyy, Viscous flow computations with the method of lattice Boltzmann equation, Progress in Aerospace Sciences 39 (5) (2003) 329–367. doi:10.1016/S0376-0421(03)00003-4.

[8] I. Ginzburg, D. d'Humières, Multireflection boundary conditions for lattice Boltzmann models, Phys. Rev. E 68 (2003) 066614. doi:10.1103/PhysRevE.68.066614.
URL `https://journals.aps.org/pre/abstract/10.1103/PhysRevE.68.066614`

[9] O. Filippova, D. Hänel, Grid refinement for lattice-BGK models, J. Comput. Phys. 147 (1) (1998) 219–228. doi:10.1006/jcph.1998.6089.

[10] R. Mei, L. Luo, W. Shyy, An accurate curved boundary treatment in the lattice Boltzmann method, J. Comput. Phys. 155 (2) (1999) 307–330. doi:10.1006/jcph.1999.6334.

[11] Z. Guo, C. Zheng, B. Shi, An extrapolation method for boundary conditions in lattice Boltzmann method, Phys. Fluids 14 (6) (2002) 2007–2010. doi:10.1063/1.1471914.

[12] D. Noble, J. Torczynski, A lattice Boltzmann method for partially saturated computational cells, Int. J. Mod. Phys. C 9 (8) (1998) 1189–1201. doi:10.1142/S0129183198001084.

[13] Q. Zou, X. He, On pressure and velocity boundary conditions for the lattice Boltzmann BGK model, Phys. Fluids 9 (6) (1997) 1591–1598. doi:10.1006/jcph.1999.6334.

[14] J. Wu, C. Shu, An improved immersed boundary-lattice Boltzmann method for simulating three-dimensional incompressible flows, J. Comput. Phys. 229 (2010) 5022–5042. doi:10.1016/j.jcp.2010.03.024.

[15] J. Favier, A. Revel, A. Pinelli, A lattice Boltzmann-immersed boundary method to simulate the fluid interaction with moving and slender flexible objects, J. Comput. Phys. 261 (2014) 145–161. doi:10.1016/j.jcp.2013.12.052.

[16] A. Delouei, M. Nazari, M. Kayhani, G. Ahmadi, A non-Newtonian direct numerical study for stationary and moving objects with various shapes: An immersed boundary lattice Boltzmann approach, J. Aerosol Sci. 93 (2016) 45–62. doi:10.1016/j.jaerosci.2015.11.006.

[17] R. Huang, H. Wu, An immersed boundary-thermal lattice Boltzmann method for solid-liquid phase change, J. Comput. Phys. 277 (2014) 305–319. doi:10.1016/j.jcp.2014.08.020.

[18] A. De Rosis, G. Falcucci, S. Ubertini, F. Ubertini, Aeroelastic study of flexible flapping wings by a coupled lattice Boltzmann-finite element approach with immersed boundary method, J. Fluids Structures 49 (2014) 516–533. doi:10.1016/j.jfluidstructs.2014.05.010.

[19] C. Peskin, The immersed boundary method, Act. Num. 11 (2002) 479–517. doi:10.1017/S0962492902000077.

[20] M. Dupin, I. Halliday, C. Care, L. Alboul, L. Munn, Modeling the flow of dense suspensions of deformable particles in three dimensions, Phys. Review E (75) (2007) 066707. doi:10.1103/PhysRevE.75.066707.

[21] Y. Sui, Y. Chew, P. Roy, H. Low, A hybrid method to study flow-induced deformation of three-dimensional capsules, J. Comput. Phys. 227 (2008) 6351–6371. doi:doi:10.1016/j.jcp.2008.03.017.

[22] T. Krüger, F. Varnik, D. Raabe, Efficient and accurate simulations of deformable particles immersed in a fluid using a combined immersed boundary lattice Boltzmann finite element method, Comput. Math. Appl. 61 (2011) 3485–3505. doi:doi:10.1016/j.camwa.2010.03.057.

[23] Z. Feng, E. Michaelides, The immersed boundary lattice Boltzmann method for solving fluid-particles interaction problems, J. Comput. Phys. 195 (2004) 602–628. doi:10.1016/j.jcp.2003.10.013.

[24] A. ten Cate, C. Nieuwstad, J. Derksen, H. Van den Akker, Particle imaging velocimetry experiments and lattice Boltzmann simulations on a single sphere settling under gravity, Phys. Fluids 14 (11) (2002) 4012–4025. doi:10.1063/1.1512918.

[25] Z. Feng, E. Michaelides, Proteus: a direct forcing method in the simulations of particulate flows, J. Comput. Phys. 202 (1) (2005) 20–51. doi:10.1016/j.jcp.2004.06.020.

[26] A. Dupuis, P. Chatelain, P. Koumoutsakos, An immersed boundary lattice Boltzmann method for the simulation of the flow past an impulsively started cylinder, J. Comput. Phys. 227 (9) (2008) 4486–4498. doi:10.1016/j.jcp.2008.01.009.

[27] E. A. Fadlun, R. Verzicco, Y. P. Orl, J. Mohd-Yusof, Combined immersed-boundary finite difference methods for three-dimensional complex flow simulations, J. Comput. Phys. (2000) 35–60doi:10.1006/jcph.2000.6484.

[28] J. Wu, C. Shu, Implicit velocity correction-based immersed boundary-lattice Boltzmann method and its applications, J. Comput. Phys. 228 (6) (2009) 1963–1979. doi:10.1016/j.jcp.2008.11.019.

[29] M. Meldi, E. Vergnault, P. Sagaut, An arbitrary Lagrangian–Eulerian approach for the simulation of immersed moving solids with lattice Boltzmann method, J. Comput. Phys. 235 (2013) 182–198. doi:10.1016/j.jcp.2012.10.014.

[30] T. Hughes, W. Liu, T. Zimmermann, Lagrangian-Eulerian finite element formulation for incompressible viscous flows, Comput. Methods Appl. Mech. Eng. 29 (1981) 329–349. doi:10.1016/0045-7825(81)90049-9.

[31] J. Donea, A. Huerta, J. Ponthot, A. Rodriguez-Ferran, Arbitrary Lagrangian Eulerian methods, in: Encyclopedia of Computational Mechanics, John Wiley & Sons, Ltd, 2004. doi:10.1002/0470091355.ecm009.

[32] X. Shi, N. Phan-Thien, Distributed Lagrange multiplier/fictitious domain method in the framework of lattice Boltzmann method for fluid–structure interactions, J. Comput. Phys. 206 (1) (2005) 81–94. doi:10.1016/j.jcp.2004.12.017.

[33] R. Glowinski, T. W. Pan, T. I. Hesla, D. D. Joseph, A distributed Lagrange multiplier/fictitious domain method for particulate flows, Int. J. Multiphase Flow 25 (5) (1999) 755–794. doi:10.1016/S0301-9322(98)00048-2.

[34] Z. Yu, A DLM/FD method for fluid/flexible-body interactions, J. Comput. Phys. 207 (1) (2005) 1–27. doi:10.1016/j.jcp.2004.12.026.

[35] S. Tao, J. Hu, Z. Guo, An investigation on momentum exchange methods and refilling algorithms for lattice boltzmann simulation of particulate flows, Comput. Fluids 133 (2016) 1–14. doi:10.1016/j.compfluid.2016.04.009.

[36] M. Souli, J. Zolesio, Arbitrary Lagrangian-Eulerian and free surface methods in fluid mechanics, Comput. Methods Appl. Mech. Eng. 191 (2001) 451–466. doi:10.1016/S0045-7825(01)00313-9.

[37] P. Angot, C. Bruneau, P. Fabrie, A penalization method to take into account obstacles in incompressible viscous flows, Numer. Math. 81 (4) (1999) 497–520. doi:10.1016/j.jcp.2012.01.036.

[38] B. Maury, Numerical analysis of a finite element/volume penalty method, SIAM J. Numer. Anal. 47 (2) (2009) 1126–1148.

[39] D. Kolomenskiy, K. Schneider, A Fourier spectral method for the Navier-Stokes equations with volume penalization for moving solid obstacles, J. Comput. Phys. 228 (2009) 5687–5709. doi:doi:10.1016/j.jcp.2009.04.026.

[40] J. Morales, M. Leroy, W. Bos, K. Schneider, Simulation of confined magnetohydrodynamic flows with Dirichlet boundary conditions using a pseudo-spectral method with volume penalization, J. Comput. Phys. 274 (2014) 64–94. doi:10.1016/j.jcp.2014.05.038.

[41] B. Kadoch, T. Reimann, K. Schneider, M. Schafer, Comparison of a spectral method with volume penalization and a finite volume method with body fitted grids for turbulent flows, Comput. Fluids 133 (2016) 140–150. doi:10.1016/j.compfluid.2016.04.028.

[42] M. Benamour, E. Liberge, C. Béghein, Lattice Boltzmann method for fluid flow around bodies using volume penalization, Int. J. Multiphys. 9 (3) (2015) 299–316. doi:10.1260/1750-9548.9.3.299.

[43] M. Benamour, Développement d'une méthode de pénalisation volumique en lattice Boltzmann: Application aux domaines mobiles, Ph.D. thesis, Université de La Rochelle, France (2015).

[44] Z. Guo, C. Zheng, B. Shi, Discrete lattice effects on the forcing term in the lattice Boltzmann method, Phys. Rev. E 65 (4) (2002) 046308. doi:10.1103/PhysRevE.65.046308.

[45] D. d'Humières, Generalized lattice Boltzmann equations, In: Shizgal BD, Weaver DP, editors. Rarefied Gas Dynamics:Theory and Simulations, Progress in Astronautics and Aeronautics 159 (1992) 450–458. doi:10.2514/5.9781600866319.0450.0458.

[46] J. Lu, H. Han, B. Shi, Z. Guo, Immersed boundary lattice Boltzmann model based on multiple relaxation times, Phys. Rev. E 85 (1) (2012) 016711. doi:10.1103/PhysRevE.85.016711.
URL `https://journals.aps.org/pre/abstract/10.1103/PhysRevE.85.016711`

[47] G. Le, J. Zhang, Boundary slip from the immersed boundary lattice Boltzmann models, Phys. Rev. E 79 (2009) 026701. doi:10.1103/PhysRevE.79.026701.
URL `https://journals.aps.org/pre/abstract/10.1103/PhysRevE.79.026701`

[48] S. Farnoush, M. Manzari, Comparison of boundary slip for two variants of immersed boundary method in lattice Boltzmann framework, Physica A 404 (2014) 200–216. doi:10.1016/j.physa.2014.02.010.

[49] Z. Yang, Lattice Boltzmann outflow treatments: Convective conditions and others, Comput. Math. Appl. 65 (2013) 160–171. doi:10.1016/j.camwa.2012.11.012.

[50] B. Wen, C. Zhang, Y. Tu, C. Wang, H. Fang, Galilean invariant fluid–solid interfacial dynamics in lattice Boltzmann simulations, J. Comput. Phys. 266 (2014) 161 – 170. doi:10.1016/j.jcp.2014.02.018.

[51] C. Wen, C. Lin, Two-dimensional vortex shedding of a circular cylinder, Phys. Fluids 13 (2001) 557–560. doi:10.1063/1.1338544.

[52] C. Wen, C. Yeh, M. Wang, C. Lin, On the drag of two-dimensional flow about a circular cylinder, Phys. Fluids 16 (2004) 3828–3831. doi:10.1063/1.1789071.

[53] OpenFOAM, https://openfoam.org, 2017.

[54] D. Shiels, A. Leonard, A. Roshko, Flow-induced vibration of a circular cylinder at limiting structural parameters, J. Fluids Struct. 15 (1) (2001) 3–21. doi:10.1006/jfls.2000.0330.

[55] J. Ahrens, B. Geveci, C. Law, ParaView: An end-user tool for large-data visualization, 2005. doi:10.1016/B978-012387582-2/50038-1.

Erwan Liberge is an associate professor of numerical analysis and mechanics at the LaSIE (Laboratory of Engineering Sciences for the Environment), University of La Rochelle, France.

Claudine Béghein is an associate professor of numerical analysis and fluid mechanics at the LaSIE (Laboratory of Engineering Sciences for the Environment), University of La Rochelle, France.